

Journal of
Mechanics of
Materials and Structures

**VIBRATION SUPPRESSION ANALYSIS OF FGM SHELLS WITH
HIGHER ORDER SHEAR DEFORMATION THEORY**

Suresh Chandra Pradhan

Volume 4, N^o 1

January 2009



mathematical sciences publishers

VIBRATION SUPPRESSION ANALYSIS OF FGM SHELLS WITH HIGHER ORDER SHEAR DEFORMATION THEORY

SURESH CHANDRA PRADHAN

Analytical solutions of functionally graded material (FGM) shells with embedded magnetostrictive layers are presented in this study. These magnetostrictive layers are used for vibration suppression in the functionally graded shells. Higher order shear deformation theory is employed to study the vibration suppression characteristics. The exact solution for the FGM shell with simply supported boundary conditions is based on the Navier solution procedure. Negative velocity feedback control is used. The parametric effect of the location of the magnetostrictive layers, material properties, and control parameters on the suppression effect are investigated in detail. Higher order shear deformation theory has significant influence on the prediction of the vibration response of thick shells. Further, it is found that the shortest vibration suppression time is achieved by placing the actuating layers farthest from the neutral plane, that the use of thinner smart material layers leads to better vibration attenuation characteristics, and that the vibration suppression time is longer for a smaller value of the feedback control coefficient.

A list of symbols can be found starting on page 54.

1. Introduction

A number of materials have been used in sensor/actuator applications. Piezoelectric materials, magnetostrictive materials, shape memory alloys, and electrorheological fluids have all been integrated with structures to make smart structures. Among these materials piezoelectric, electrostrictive, and magnetostrictive materials have the capability to serve as both sensors and actuators. Piezoelectric materials exhibit a linear relationship between the electric field and strains for low field values (up to 100 V/mm). This relationship is nonlinear for large fields, and the material exhibits hysteresis. Further, piezoelectric materials show dielectric aging and hence lack reproducibility of strains, that is, a drift from zero state of strain is observed under cyclic electric field applications.

An ideal actuator, for distributed embedded application, should have high energy density, negligible weight, and point excitation with a wide frequency bandwidth. Terfenol-D, a magnetostrictive material, has the characteristics of being able to produce strains up to 2000 and an energy density as high as 0.0025 J m^{-3} in response to a magnetic field. Goodfriend and Shoop [1992] reviewed the material properties of Terfenol-D with regard to its use in vibration isolation. Anjanappa and Bi [1994] investigated the feasibility of using embedded magnetostrictive mini actuators for smart structure applications, such as vibration suppression of beams. Bryant et al. [1993] presented experimental results of a magnetostrictive Terfenol-D rod used in dual capacity as a passive structural support element and an active vibration control actuator. Krishna Murty et al. [1997] proposed magnetostrictive actuators that take advantage of the ease with which the actuators can be embedded and the use of the remote excitation capability of

Keywords: functionally graded materials, higher order, shear deformation, vibration, shell.

magnetostrictive particles as new actuators for smart structures. This work is limited to flexible beam theory.

Friedmann et al. [2001] used the magnetostrictive material Terfenol-D in high speed helicopter rotors and studied the vibration reduction characteristics. Vibration and shape control of flexible structures are achieved with the help of actuators and a control law. The response of functionally graded material (FGM) shells is also studied by Loy et al. [1999], Pradhan et al. [2000], Woo and Meguid [2001], and He et al. [2002]. Many modern techniques have been developed in recent years to meet the challenge of designing controllers that suit the function under the required conditions. There have been a number of studies on vibration control of flexible structures using magnetostrictive materials [Bryant et al. 1993; Anjanappa and Bi 1994; Krishna Murty et al. 1997; Giurgiutiu et al. 2001; Pradhan et al. 2001]. Higher order shear deformation theory (HSDT) is discussed in [Reddy 1984a; 1984b]. Kadoli and Ganesan [2006], Haddadpour et al. [2007], Li [2008], Pradyumna and Bandyopadhyay [2008], and Matsunaga [2009] described various vibration analyses of functionally graded materials. Although there have been important research efforts devoted to characterizing the properties of Terfenol-D, fundamental information about the variation in elastomagnetic material properties in a thick functionally graded shell is not available.

In the present work vibration control of functionally graded shells is studied using HSDT. Exact solutions are developed for simply supported doubly curved functionally graded shells with magnetostrictive layers. This closed form solution exists for FGM shells where the coefficients A_{16} , A_{26} , B_{16} , B_{26} , D_{16} , D_{26} , and A_{45} are equal to zero. A simple negative velocity feedback control is used to actively control the dynamic response of the structure through a closed loop control. Numerical results of the vibration suppression effect for various locations of the magnetostrictive layers, material properties, and control parameters are presented. The influence of HSDT on thick FGM shells is also investigated.

2. Theoretical formulation

Kinematic description. Figure 1, left, shows a differential element of a doubly curved shell element with constant curvatures along two coordinate directions (ξ_1, ξ_2) , where (ξ_1, ξ_2, ζ) denote the orthogonal curvilinear coordinates such that the ξ_1 and ξ_2 curves are the lines of curvature on the middle surface ($\zeta = 0$). Thus, in the doubly curved shell panel considered here, the lines of the principal curvature coincide with the coordinate lines. The values of the principal radii of curvature of the middle surface are denoted by R_1 and R_2 . The position vector of a point $(\xi_1, \xi_2, 0)$ on the middle surface is denoted by \mathbf{r} , and the position of an arbitrary point (ξ_1, ξ_2, ζ) is denoted by \mathbf{R} (see Figure 1, top right). The square of the distance ds between points $(\xi_1, \xi_2, 0)$ and $(\xi_1 + d\xi_1, \xi_2 + d\xi_2, 0)$ is determined as [Pradhan 2005]

$$(ds)^2 = d\mathbf{r} \cdot d\mathbf{r} = \alpha_1^2 (d\xi_1)^2 + \alpha_2^2 (d\xi_2)^2, \quad (1)$$

in which $d\mathbf{r} = \mathbf{g}_1 d\xi_1 + \mathbf{g}_2 d\xi_2$, the vectors \mathbf{g}_1 and \mathbf{g}_2 ($\mathbf{g}_i = \partial \mathbf{r} / \partial \xi_i$) are tangent to the ξ_1 and ξ_2 coordinate lines and α_1, α_2 are the surface metrics:

$$\alpha_1^2 = \mathbf{g}_1 \cdot \mathbf{g}_1, \quad \alpha_2^2 = \mathbf{g}_2 \cdot \mathbf{g}_2 \quad (2)$$

The square of the distance dS between (ξ_1, ξ_2, ζ) and $(\xi_1 + d\xi_1, \xi_2 + d\xi_2, \zeta + d\zeta)$ is given by

$$(dS)^2 = d\mathbf{R} \cdot d\mathbf{R} = L_1^2 (d\xi_1)^2 + L_2^2 (d\xi_2)^2 + L_3^2 (d\zeta)^2, \quad (3)$$

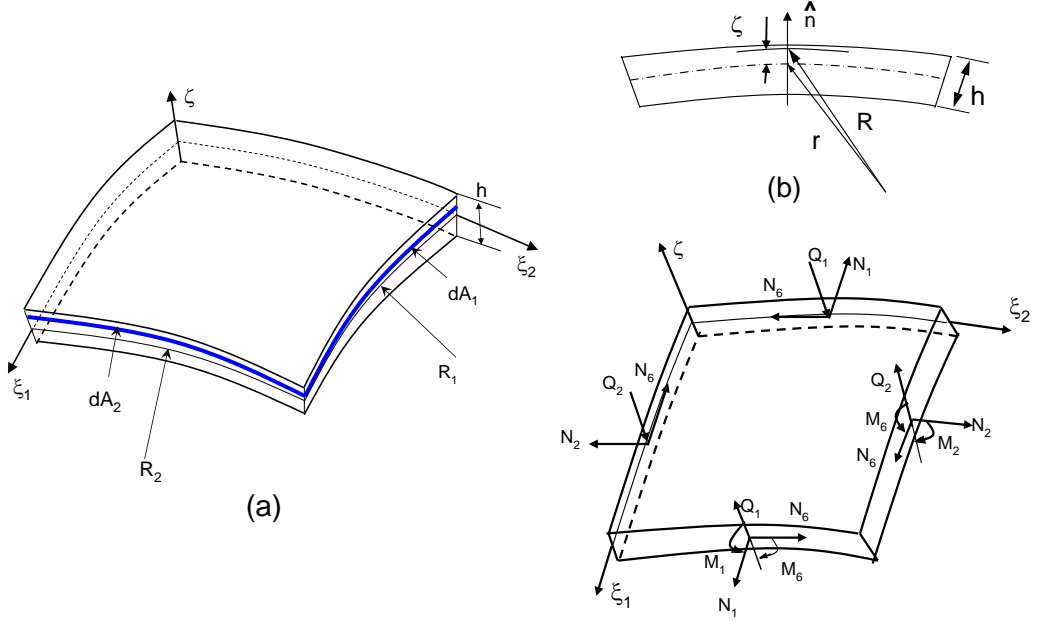


Figure 1. Geometry and stress resultants of a doubly curved shell.

in which $d\mathbf{R} = \frac{\partial \mathbf{R}}{\partial \xi_1} d\xi_1 + \frac{\partial \mathbf{R}}{\partial \xi_2} d\xi_2 + \frac{\partial \mathbf{R}}{\partial \zeta} d\zeta$ and L_1 , L_2 , and L_3 are the Lamé coefficients

$$L_1 = \alpha_1 \left(1 + \frac{\zeta}{R_1} \right), \quad L_2 = \alpha_2 \left(1 + \frac{\zeta}{R_2} \right), \quad L_3 = 1. \quad (4)$$

Displacement field. We assume the following form of the displacement field, consistent with the assumptions of a thick shell theory as explained in [Reddy and Liu 1985]:

$$\begin{aligned} \bar{u}_1(\xi_1, \xi_2, \zeta, t) &= \frac{L_1}{\alpha_1} u_1(\xi_1, \xi_2, t) + \zeta \phi_1(\xi_1, \xi_2, t) - C_1 \zeta^3 \left(\phi_1 + \frac{\partial u_3}{\alpha_1 \partial \xi_1} \right), \\ \bar{u}_2(\xi_1, \xi_2, \zeta, t) &= \frac{L_2}{\alpha_2} u_2(\xi_1, \xi_2, t) + \zeta \phi_2(\xi_1, \xi_2, t) - C_1 \zeta^3 \left(\phi_2 + \frac{\partial u_3}{\alpha_1 \partial \xi_2} \right), \\ \bar{u}_3(\xi_1, \xi_2, \zeta, t) &= u_3(\xi_1, \xi_2, t), \end{aligned} \quad (5)$$

where

$$\frac{1}{\partial x_i} = \frac{1}{\alpha_i} \frac{1}{\partial \xi_i} \quad (i = 1, 2), \quad (6)$$

$(\bar{u}_1, \bar{u}_2, \bar{u}_3)$ are the displacements of a point (ξ_1, ξ_2, ζ) along the (ξ_1, ξ_2, ζ) coordinates, and (u_1, u_2, u_3) are the displacements of a point $(\xi_1, \xi_2, 0)$ on the mid surface of the shell. C_1 is a constant, which depends on shell thickness. The strain-displacement relations are written as

$$\begin{Bmatrix} \varepsilon_1 \\ \varepsilon_2 \\ \varepsilon_6 \end{Bmatrix} = \begin{Bmatrix} \varepsilon_1^0 \\ \varepsilon_2^0 \\ \varepsilon_6^0 \end{Bmatrix} + \zeta \begin{Bmatrix} \varepsilon_1^1 \\ \varepsilon_2^1 \\ \varepsilon_6^1 \end{Bmatrix} + \zeta^3 \begin{Bmatrix} \varepsilon_1^2 \\ \varepsilon_2^2 \\ \varepsilon_6^2 \end{Bmatrix}, \quad \begin{Bmatrix} \gamma_4 \\ \gamma_5 \end{Bmatrix} = \begin{Bmatrix} \gamma_4^0 \\ \gamma_5^0 \end{Bmatrix} + \zeta^2 \begin{Bmatrix} \gamma_4^1 \\ \gamma_5^1 \end{Bmatrix}, \quad (7)$$

where

$$\begin{aligned} \begin{Bmatrix} \varepsilon_1^0 \\ \varepsilon_2^0 \\ \varepsilon_6^0 \end{Bmatrix} &= \begin{Bmatrix} \frac{\partial u_1}{\partial x_1} + \frac{1}{R_1} u_3 \\ \frac{\partial u_2}{\partial x_2} + \frac{1}{R_2} u_3 \\ \frac{\partial u_2}{\partial x_1} + \frac{\partial u_1}{\partial x_2} \end{Bmatrix}, & \begin{Bmatrix} \varepsilon_1^1 \\ \varepsilon_2^1 \\ \varepsilon_6^1 \end{Bmatrix} &= \begin{Bmatrix} \frac{\partial \phi_1}{\partial x_1} \\ \frac{\partial \phi_2}{\partial x_2} \\ \frac{\partial \phi_2}{\partial x_1} + \frac{\partial \phi_1}{\partial x_2} \end{Bmatrix}, & \begin{Bmatrix} \varepsilon_1^2 \\ \varepsilon_2^2 \\ \varepsilon_6^2 \end{Bmatrix} &= -C_1 \begin{Bmatrix} \frac{\partial \phi_1}{\partial x_1} + \frac{\partial^2 u_3}{\partial x_1^2} \\ \frac{\partial \phi_2}{\partial x_2} + \frac{\partial^2 u_3}{\partial x_2^2} \\ \frac{\partial \phi_2}{\partial x_1} + \frac{\partial \phi_1}{\partial x_2} + 2 \frac{\partial^2 u_3}{\partial x_1 \partial x_2} \end{Bmatrix}, \\ \begin{Bmatrix} \gamma_4^0 \\ \gamma_5^0 \end{Bmatrix} &= \begin{Bmatrix} \phi_2 + \frac{\partial u_3}{\partial x_2} \\ \phi_1 + \frac{\partial u_3}{\partial x_1} \end{Bmatrix}, & \begin{Bmatrix} \gamma_4^1 \\ \gamma_5^1 \end{Bmatrix} &= -C_2 \begin{Bmatrix} \phi_2 + \frac{\partial u_3}{\partial x_2} \\ \phi_1 + \frac{\partial u_3}{\partial x_1} \end{Bmatrix}, \end{aligned} \quad (8)$$

and (ϕ_1, ϕ_2) are rotations of a transverse normal line about the ζ_2 and ζ_1 coordinate axes, respectively:

$$\phi_1 = -\frac{\partial u_3}{\partial \zeta_1}, \quad \phi_2 = -\frac{\partial u_3}{\partial \zeta_2}. \quad (9)$$

The constants C_1 and C_2 are defined as

$$C_1 = \frac{4}{3h^2}, \quad C_2 = 3C_1. \quad (10)$$

Constitutive relations. Suppose that the shell is composed of N functionally graded layers. The stress-strain relations of the k -th layer, whether structural layer or actuating/sensing layer, in the shell coordinate system are given as

$$\begin{Bmatrix} \sigma_1 \\ \sigma_2 \\ \sigma_4 \\ \sigma_5 \\ \sigma_6 \end{Bmatrix}^{(k)} = \begin{bmatrix} Q_{11} & Q_{12} & 0 & 0 & 0 \\ Q_{12} & Q_{22} & 0 & 0 & 0 \\ 0 & 0 & Q_{44} & 0 & 0 \\ 0 & 0 & 0 & Q_{55} & 0 \\ 0 & 0 & 0 & 0 & Q_{66} \end{bmatrix}^{(k)} \begin{Bmatrix} \varepsilon_1 \\ \varepsilon_2 \\ \varepsilon_4 \\ \varepsilon_5 \\ \varepsilon_6 \end{Bmatrix} - \zeta \begin{Bmatrix} ce_{31} \\ e_{32} \\ 0 \\ 0 \\ e_{36} \end{Bmatrix}^{(k)} H, \quad (11)$$

where $Q_{ij}^{(k)}$ are the stiffnesses of the k -th layer and

$$Q_{11} = \frac{E_{\text{FGM}}}{1 - \nu_{\text{FGM}}^2}, \quad Q_{12} = \frac{\nu_{\text{FGM}} E_{\text{FGM}}}{1 - \nu_{\text{FGM}}^2}, \quad Q_{22} = Q_{11}, \quad Q_{44} = Q_{55} = Q_{66} = G_{\text{FGM}}. \quad (12)$$

The superscript k on Q_{ij} as well as on the engineering constants E_{FGM} , ν_{FGM} , and so on are omitted for brevity. In Equation (11), H denotes the intensity of the magnetic field. H is applied normal to the thickness of the shell. e_{ij} are the magnetostrictive material coefficients.

Feedback control. A velocity feedback control is used in the present study. In the velocity feedback control, the magnetic field intensity H is expressed in terms of the coil current $I(\zeta_1, \zeta_2, t)$ as

$$H(\zeta_1, \zeta_2, t) = k_c I(\zeta_1, \zeta_2, t). \quad (13)$$

Current I is related to the transverse velocity \dot{u}_3 component as

$$I(\zeta_1, \zeta_2, t) = c(t) \frac{\partial u_3}{\partial t} \quad (14)$$

where k_c is the magnetic coil constant and is related to the number of coil turns n_c , the coil width b_c , and the coil radius r_c by

$$k_c = \frac{n_c}{\sqrt{b_c^2 + 4r_c^2}}. \quad (15)$$

The parameter $c(t)$ is known as the control gain.

Equations of motion. The equations of motion are derived from the dynamic version of the principle of virtual work. By integrating the displacement gradients by parts and setting the coefficients δu_1 , δu_2 , δu_3 , $\delta \phi_1$, and $\delta \phi_2$ to zero separately (the moment terms in the first two equations are omitted) we get

$$\begin{aligned} \frac{\partial N_1}{\partial x_1} + \frac{\partial N_6}{\partial x_2} &= \bar{I}_1 \frac{\partial^2 u_1}{\partial t^2} + \bar{I}_2 \frac{\partial^2 \phi_1}{\partial t^2} - \bar{I}_3 \frac{\partial^2 u_3}{\partial t^2}, & \frac{\partial N_6}{\partial x_1} + \frac{\partial N_2}{\partial x_2} &= \bar{J}_1 \frac{\partial^2 u_2}{\partial t^2} + \bar{J}_2 \frac{\partial^2 \phi_2}{\partial t^2} - \bar{J}_3 \frac{\partial^2 u_3}{\partial t^2}, \\ \frac{\partial Q_1}{\partial x_1} + \frac{\partial Q_2}{\partial x_2} - C_2 \left(\frac{\partial K_1}{\partial x_1} + \frac{\partial K_2}{\partial x_2} \right) + C_1 \left(\frac{\partial^2 P_1}{\partial x_1^2} + 2 \frac{\partial^2 P_6}{\partial x_1 \partial x_2} + \frac{\partial^2 P_2}{\partial x_2^2} \right) - \frac{N_1}{R_1} - \frac{N_2}{R_2} + q \\ &= \bar{I}_3 \frac{\partial^3 u_1}{\partial x_1 \partial t^2} + \bar{I}_5 \frac{\partial^3 \phi_1}{\partial x_1 \partial t^2} + \bar{J}_3 \frac{\partial^3 u_2}{\partial x_2 \partial t^2} + \bar{J}_5 \frac{\partial^3 \phi_2}{\partial x_2 \partial t^2} + I_1 \frac{\partial^2 u_3}{\partial t^2} - C_1^2 I_7 \left(\frac{\partial^4 u_3}{\partial x_1^2 \partial t^2} + \frac{\partial^4 u_3}{\partial x_2^2 \partial t^2} \right), \\ \frac{\partial M_1}{\partial x_1} + \frac{\partial M_6}{\partial x_2} - Q_1 + C_2 K_1 - C_1 \left(\frac{\partial P_1}{\partial x_1} + \frac{\partial P_6}{\partial x_2} \right) &= \bar{I}_2 \frac{\partial^2 u_1}{\partial t^2} + \bar{I}_4 \frac{\partial^2 \phi_1}{\partial t^2} - \bar{I}_5 \frac{\partial^3 u_3}{\partial x_1 \partial t^2}, \\ \frac{\partial M_6}{\partial x_1} + \frac{\partial M_2}{\partial x_2} - Q_2 + C_2 K_2 - C_1 \left(\frac{\partial P_6}{\partial x_1} + \frac{\partial P_2}{\partial x_2} \right) &= \bar{J}_2 \frac{\partial^2 u_2}{\partial t^2} + \bar{J}_4 \frac{\partial^2 \phi_2}{\partial t^2} - \bar{J}_5 \frac{\partial^3 u_3}{\partial x_2 \partial t^2}, \end{aligned} \quad (16)$$

where the forces N_i , the moments M_i , the third-order moments P_i , and the shear forces Q_1 , Q_2 , K_1 , and K_2 are defined as

$$\begin{aligned} (N_i, M_i, P_i) &= \sum_{k=1}^N \int_{\zeta_{k-1}}^{\zeta_k} \sigma_i^{(k)}(1, \zeta, \zeta^3) d\zeta \quad (i = 1, 2, 6), \\ (Q_1, K_1) &= \sum_{k=1}^N \int_{\zeta_{k-1}}^{\zeta_k} \sigma_5^{(k)}(1, \zeta^2) d\zeta, \quad (Q_2, K_2) = \sum_{k=1}^N \int_{\zeta_{k-1}}^{\zeta_k} \sigma_4^{(k)}(1, \zeta^2) d\zeta. \end{aligned} \quad (17)$$

The inertia-driven terms \bar{I}_i and \bar{J}_i are defined as

$$\begin{aligned} \bar{I}_1 &= I_1 + \frac{2}{R_1} I_2, & \bar{I}_2 &= I_3 + \frac{1}{R_1} I_3 - C_1 \left(I_4 + \frac{1}{R_1} I_5 \right), & \bar{I}_3 &= C_1 \left(I_4 + \frac{1}{R_1} I_5 \right), \\ \bar{J}_1 &= I_1 + \frac{2}{R_2} I_2, & \bar{J}_2 &= I_3 + \frac{1}{R_2} I_3 - C_1 \left(I_4 + \frac{1}{R_2} I_5 \right), & \bar{J}_3 &= C_1 \left(I_4 + \frac{1}{R_2} I_5 \right), \\ \bar{I}_4 &= I_3 - C_1 (2I_5 - C_1 I_7), & \bar{I}_5 &= C_1 (2I_5 - C_1 I_7), & \bar{J}_4 &= \bar{I}_4, \quad \bar{J}_5 = \bar{I}_5. \end{aligned} \quad (18)$$

The inertia terms are defined as

$$(I_1, I_2, I_3, I_4, I_5, I_7) = \sum_{k=1}^N \int_{\zeta_{k-1}}^{\zeta_k} \rho^{(k)}(1, \zeta, \zeta^2, \zeta^3, \zeta^4, \zeta^6) d\zeta, \quad (19)$$

where $\rho^{(k)}$ is the density of the k -th layer and N is the number of layers in the laminate.

Shell constitutive equation. Using Equations (7) and (11) in (17) we get the following constitutive equations for the actuator embedded shell:

$$\begin{Bmatrix} \{N\} \\ \{M\} \\ \{P\} \end{Bmatrix} = \begin{bmatrix} [A] & [B] & [E] \\ [B] & [D] & [F] \\ [E] & [F] & [H] \end{bmatrix} \begin{Bmatrix} \{\varepsilon^0\} \\ \{\varepsilon^1\} \\ \{\varepsilon^2\} \end{Bmatrix} - \begin{Bmatrix} \{N\} \\ \{M\} \\ \{P\} \end{Bmatrix}^M, \quad \begin{Bmatrix} \{Q\} \\ \{K\} \end{Bmatrix} = \begin{bmatrix} [A] & [D] \\ [D] & [F] \end{bmatrix} \begin{Bmatrix} \{\gamma^0\} \\ \{\gamma^1\} \end{Bmatrix} - \begin{Bmatrix} \{Q\} \\ \{K\} \end{Bmatrix}^M, \quad (20)$$

where the shell stiffness coefficients (A_{ij} , B_{ij} , D_{ij} , E_{ij} , F_{ij} , and H_{ij} for $i, j = 1, 2, 6$) are defined by

$$(A_{ij}, B_{ij}, D_{ij}, E_{ij}, F_{ij}, H_{ij}) = \sum_{k=1}^N \int_{\zeta_k}^{\zeta_{k+1}} \bar{Q}_{ij}^{(k)}(1, \zeta, \zeta^2, \zeta^3, \zeta^4, \zeta^6) d\zeta \quad (21)$$

and the shell stiffness coefficients (A_{ij} , D_{ij} , and F_{ij} for $i, j = 4, 5$) are defined by

$$(A_{ij}, D_{ij}, F_{ij}) = \sum_{k=1}^N \int_{\zeta_k}^{\zeta_{k+1}} \bar{Q}_{ij}^{(k)}(1, \zeta^2, \zeta^4) d\zeta \quad (i, j = 4, 5). \quad (22)$$

The magnetostrictive stress resultants ($\{N_i^M\}$, $\{M_i^M\}$, and $\{K_i^M\}$ for $i = 1, 2$) are defined by

$$\begin{aligned} \begin{Bmatrix} N_1^M \\ N_2^M \end{Bmatrix} &= \sum_{k=m_1, m_2, \dots}^N \int_{\zeta_k}^{\zeta_{k+1}} \begin{Bmatrix} \bar{e}_{31} \\ \bar{e}_{32} \end{Bmatrix} H_\zeta d\zeta = ck_c \sum_{k=m_1, m_2, \dots}^N \int_{\zeta_k}^{\zeta_{k+1}} \begin{Bmatrix} \bar{e}_{31} \\ \bar{e}_{32} \end{Bmatrix} \frac{\partial u_3}{\partial t} d\zeta \equiv \begin{Bmatrix} \mathcal{A}_{31} \\ \mathcal{A}_{32} \end{Bmatrix} \frac{\partial u_3}{\partial t}, \\ \begin{Bmatrix} M_1^M \\ M_2^M \end{Bmatrix} &= \sum_{k=m_1, m_2, \dots}^N \int_{\zeta_k}^{\zeta_{k+1}} \begin{Bmatrix} \bar{e}_{31} \\ \bar{e}_{32} \end{Bmatrix} \zeta H_\zeta d\zeta = ck_c \sum_{k=m_1, m_2, \dots}^N \int_{\zeta_k}^{\zeta_{k+1}} \begin{Bmatrix} \bar{e}_{31} \\ \bar{e}_{32} \end{Bmatrix} \frac{\partial u_3}{\partial t} \zeta d\zeta \equiv \begin{Bmatrix} \mathcal{B}_{31} \\ \mathcal{B}_{32} \end{Bmatrix} \frac{\partial u_3}{\partial t}, \\ \begin{Bmatrix} K_1^M \\ K_2^M \end{Bmatrix} &= \sum_{k=m_1, m_2, \dots}^N \int_{\zeta_k}^{\zeta_{k+1}} \begin{Bmatrix} \bar{e}_{31} \\ \bar{e}_{32} \end{Bmatrix} \zeta^3 H_\zeta d\zeta = ck_c \sum_{k=m_1, m_2, \dots}^N \int_{\zeta_k}^{\zeta_{k+1}} \begin{Bmatrix} \bar{e}_{31} \\ \bar{e}_{32} \end{Bmatrix} \frac{\partial u_3}{\partial t} \zeta^3 d\zeta \equiv \begin{Bmatrix} \mathcal{C}_{31} \\ \mathcal{C}_{32} \end{Bmatrix} \frac{\partial u_3}{\partial t}, \end{aligned} \quad (23)$$

where

$$\begin{aligned} \mathcal{A}_{ij} &= ck_c \sum_{k=m_1, m_2, \dots} \bar{e}_{ij}^{(k)} (\zeta_{k+1} - \zeta_k), & i = 3, \quad j = 1, 2, \\ \mathcal{B}_{ij} &= \frac{1}{2} ck_c \sum_{k=m_1, m_2, \dots} \bar{e}_{ij}^{(k)} (\zeta_{k+1}^2 - \zeta_k^2), & i = 3, \quad j = 1, 2, \\ \mathcal{C}_{ij} &= \frac{1}{4} ck_c \sum_{k=m_1, m_2, \dots} \bar{e}_{ij}^{(k)} (\zeta_{k+1}^4 - \zeta_k^4), & i = 3, \quad j = 1, 2, \end{aligned} \quad (24)$$

and m_1, m_2, \dots denote the layer numbers of the magnetostrictive (or any actuating/sensing) layers.

Functionally graded material. The material properties P_{FGM} of the FGM are controlled by the volume fractions V_{fi} and the individual material properties P_i of the constituent materials:

$$P_{\text{FGM}} = \sum_{i=1}^{nm} P_i V_{fi}. \quad (25)$$

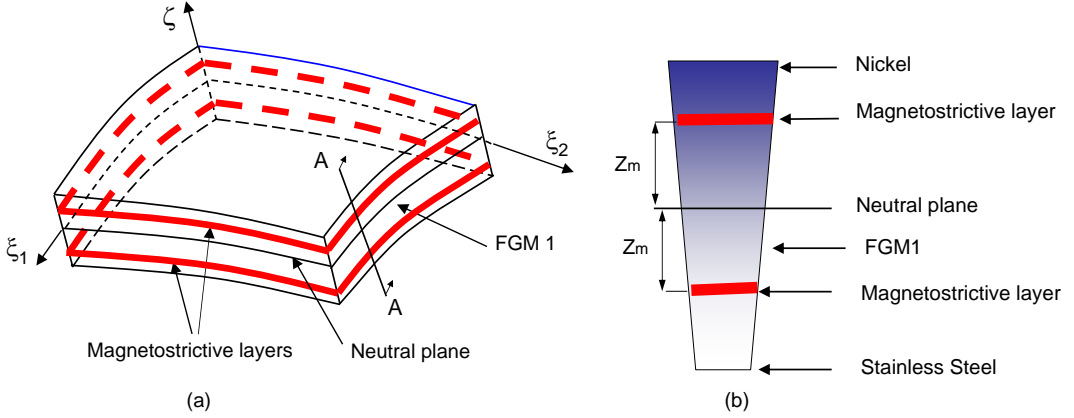


Figure 2. Left: functionally graded shell with embedded magnetostrictive layers. Right: exploded sectional view.

In the present case two different materials are particle mixed to form the FGM material. A schematic of the FGM shell with magnetostrictive layers is shown in Figure 2. The left half of the figure shows two layers of magnetostrictive materials placed symmetrically away from the neutral plane of the FGM shell. A zoomed view of section AA is shown on the right. Assuming there are no defects like voids or foreign particles in the FGM material, the sum of the volume fractions of all the constituent materials is unity:

$$\sum_{i=1}^{nm} V_{fi} = 1. \tag{26}$$

For example, metal and ceramic materials ($nm = 2$) are mixed to form the FGM shell. The volume fractions of the metal and ceramic materials are calculated by simple integration of the distribution over a domain. Different problems of interest have different expressions for the volume fractions. For bending problems of plates and shells the volume fractions of the metal (V_m) and ceramic (V_c) materials are defined as

$$V_m = \left(\frac{h-2z}{2h}\right)^{R_n}, \quad V_c = 1 - V_m, \tag{27}$$

where z is the thickness coordinate ($-h/2 \leq z \leq h/2$) and h represents the shell thickness. R_n is the power law exponent ($0 \leq R_n \leq \infty$). Here V_m varies from 100% to 0% as z varies from $-h/2$ to $h/2$. Similarly V_c varies from 0% to 100% as z varies from $-h/2$ to $h/2$. For various R_n values the average V_m and V_c are depicted in the top and bottom of Figure 3, respectively. The Young’s modulus and Poisson’s ratio of a FGM shell made up of two different materials are expressed as

$$E_{FGM} = (E_2 - E_1)\left(\frac{2z+h}{2h}\right)^{R_n} + E_1, \quad \nu_{FGM} = (\nu_2 - \nu_1)\left(\frac{2z+h}{2h}\right)^{R_n} + \nu_1. \tag{28}$$

E_1 , E_2 , and E_{FGM} are the Young’s moduli of the constituent materials and the FGM material, respectively. ν_1 , ν_2 , and ν_{FGM} are the Poisson’s ratios of the constituent materials and the FGM material, respectively. From Equation (28) we note that at $z = -h/2$, the FGM material properties are the same as those of material 1, while at $z = h/2$, they are the same as those of material 2. Thus, the FGM material properties vary smoothly across the thickness, from material 1 at the inner surface to material 2 at the outer surface.

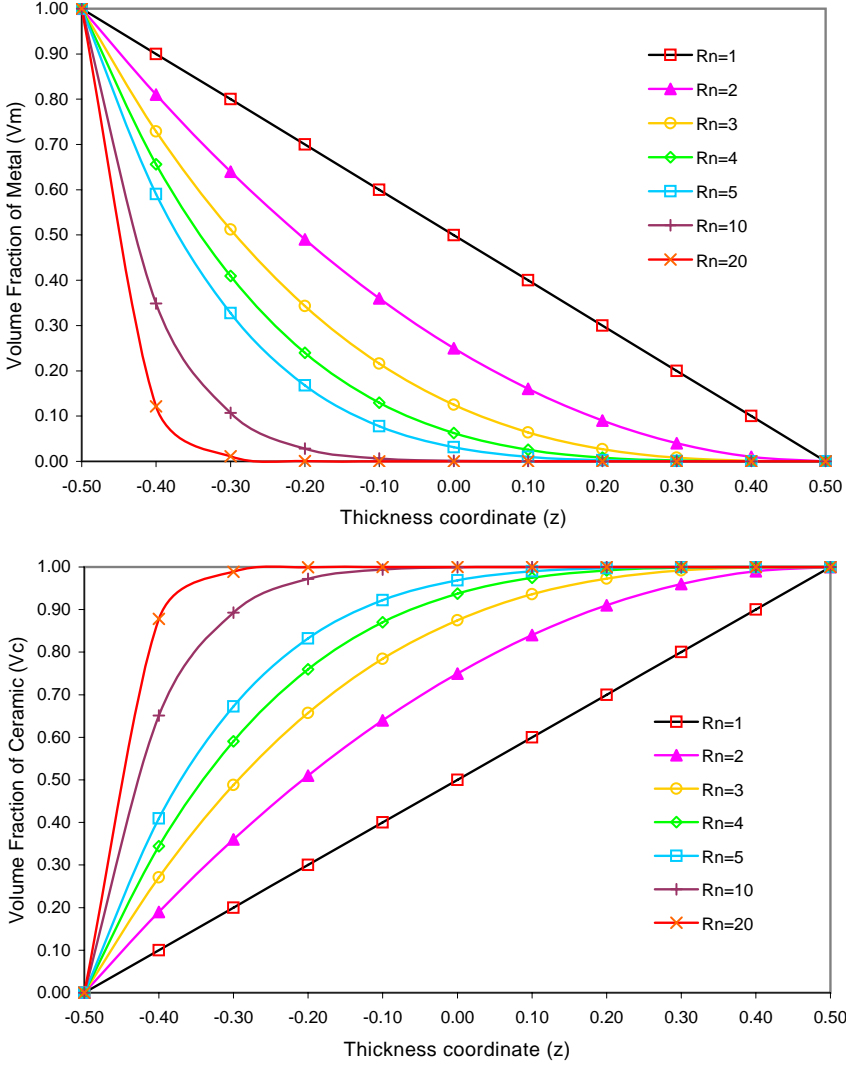


Figure 3. Volume fractions of metal and ceramic materials in the FGM shell.

Two different FGM materials are considered in the present study: FGM1 consists of stainless steel and nickel (Figure 2b), while FGM2 consists of nickel and aluminum oxide. The material properties of stainless steel, nickel, and aluminum oxide are listed in Table 1. The material properties of the FGM shells are calculated at room temperature.

	Young's Modulus E (GPa)	Poisson's ratio	Density (kg m^{-3})
Stainless steel	201.04	0.3262	7900
Nickel	244.27	0.2882	8909
Aluminum oxide	349.55	0.260	3970

Table 1. Material properties of FGM constituent materials.

3. Analytical solution

The equations of motion (16) can be expressed in terms of the displacements ($u_1, u_2, u_3, \phi_1, \phi_2$) by substituting the force and moment resultants from (20). Further, one can derive the equation of motion (16) for homogeneous shells. An exact solution for the partial differential equations (16) on arbitrary domains and for general boundary conditions is not possible. However, for simply supported shells whose projection in the x_1, x_2 -plane is a rectangle and for a lamination scheme of antisymmetric cross-ply or symmetric cross-ply type the equations (16) are solved exactly. The Navier solution exists if $A_{i6} = B_{i6} = D_{i6} = E_{i6} = F_{i6} = H_{i6} = 0$ ($i = 1, 2$), and $A_{45} = D_{45} = F_{45} = 0$ [Reddy 1984a]. The simply-supported boundary conditions for the HSDT are assumed to be

$$\begin{aligned}
 u_1(x_1, 0, t) = 0, & \quad u_1(x_1, b, t) = 0, & \quad u_2(0, x_2, t) = 0, & \quad u_2(a, x_2, t) = 0, \\
 u_3(x_1, 0, t) = 0, & \quad u_3(x_2, b, t) = 0, & \quad u_3(0, x_2, t) = 0, & \quad u_3(a, x_2, t) = 0, \\
 N_1(0, x_2, t) = 0, & \quad N_1(a, x_2, t) = 0, & \quad N_2(x_1, 0, t) = 0, & \quad N_2(x_1, b, t) = 0, \\
 M_1(0, x_2, t) = 0, & \quad M_1(a, x_2, t) = 0, & \quad M_2(x_1, 0, t) = 0, & \quad M_2(x_1, b, t) = 0, \\
 P_1(0, x_2, t) = 0, & \quad P_1(a, x_2, t) = 0, & \quad P_2(x_1, 0, t) = 0, & \quad P_2(x_1, b, t) = 0, \\
 \phi_1(x_1, 0, t) = 0, & \quad \phi_1(x_1, b, t) = 0, & \quad \phi_2(0, x_2, t) = 0, & \quad \phi_2(a, x_2, t) = 0,
 \end{aligned} \tag{29}$$

where a and b denote the lengths along the x_1 and x_2 axes, respectively. The boundary conditions in (29) are satisfied by the following expansions [Reddy 2004]:

$$\begin{aligned}
 u_1(x_1, x_2, t) &= \sum_{n=1}^{\infty} \sum_{m=1}^{\infty} U_{mn}(t) \cos \alpha x_1 \sin \beta x_2, & u_2(x_1, x_2, t) &= \sum_{n=1}^{\infty} \sum_{m=1}^{\infty} V_{mn}(t) \sin \alpha x_1 \cos \beta x_2, \\
 u_3(x_1, x_2, t) &= \sum_{n=1}^{\infty} \sum_{m=1}^{\infty} W_{mn}(t) \sin \alpha x_1 \sin \beta x_2, \\
 \phi_1(x_1, x_2, t) &= \sum_{n=1}^{\infty} \sum_{m=1}^{\infty} X_{mn}(t) \cos \alpha x_1 \sin \beta x_2, & \phi_2(x_1, x_2, t) &= \sum_{n=1}^{\infty} \sum_{m=1}^{\infty} Y_{mn}(t) \sin \alpha x_1 \cos \beta x_2.
 \end{aligned} \tag{30}$$

Substituting (30) into (16), we obtain

$$\begin{aligned}
 \begin{bmatrix} S_{11} & S_{12} & S_{13} & S_{14} & S_{15} \\ S_{21} & S_{22} & S_{23} & S_{24} & S_{25} \\ S_{31} & S_{32} & S_{33} & S_{34} & S_{35} \\ S_{41} & S_{42} & S_{43} & S_{44} & S_{45} \\ S_{51} & S_{52} & S_{53} & S_{54} & S_{55} \end{bmatrix} \begin{Bmatrix} U_{mn} \\ V_{mn} \\ W_{mn} \\ X_{mn} \\ Y_{mn} \end{Bmatrix} + \begin{bmatrix} 0 & 0 & C_{13} & 0 & 0 \\ 0 & 0 & C_{23} & 0 & 0 \\ 0 & 0 & C_{33} & 0 & 0 \\ 0 & 0 & C_{43} & 0 & 0 \\ 0 & 0 & C_{53} & 0 & 0 \end{bmatrix} \begin{Bmatrix} \dot{U}_{mn} \\ \dot{V}_{mn} \\ \dot{W}_{mn} \\ \dot{X}_{mn} \\ \dot{Y}_{mn} \end{Bmatrix} \\
 + \begin{bmatrix} M_{11} & 0 & M_{13} & M_{14} & 0 \\ 0 & M_{22} & M_{23} & 0 & M_{25} \\ M_{31} & M_{32} & M_{33} & M_{34} & M_{35} \\ M_{41} & 0 & M_{43} & M_{44} & 0 \\ 0 & M_{52} & M_{53} & 0 & M_{55} \end{bmatrix} \begin{Bmatrix} \ddot{U}_{mn} \\ \ddot{V}_{mn} \\ \ddot{W}_{mn} \\ \ddot{X}_{mn} \\ \ddot{Y}_{mn} \end{Bmatrix} = \begin{Bmatrix} 0 \\ 0 \\ Q_{mn} \\ 0 \\ 0 \end{Bmatrix}, \tag{31}
 \end{aligned}$$

$$\begin{aligned}
S_{11} &= A_{11}\alpha^2 + A_{66}\beta^2, & S_{12} &= S_{21} = A_{12}\alpha\beta + A_{66}\alpha\beta, \\
S_{13} &= S_{31} = -A_{11}\frac{1}{R_1}\alpha - A_{12}\frac{1}{R_2}\alpha - C_1E_{11}\alpha^3 - C_1E_{12}\alpha\beta^2 - C_1E_{66}2\alpha\beta^2, \\
S_{14} &= S_{41} = B_{11}\alpha^2 - C_1E_{11}\alpha^2 + B_{66}\beta^2 - C_1E_{66}\beta^2, & S_{15} &= S_{51} = B_{12}\alpha\beta - C_1E_{12}\alpha\beta + B_{66}\alpha\beta - C_1E_{66}\alpha\beta, \\
S_{22} &= A_{66}\alpha^2 + A_{22}\beta^2, & S_{23} &= S_{32} = -2C_1E_{66}\alpha^2\beta - A_{12}\frac{1}{R_1}\beta - A_{22}\frac{1}{R_2}\beta - C_1E_{12}\alpha^2\beta - C_1E_{22}\beta^3, \\
S_{24} &= S_{42} = B_{66}\alpha\beta - C_1E_{66}\alpha\beta + B_{12}\alpha\beta - C_1E_{12}\alpha\beta, & S_{25} &= S_{52} = B_{66}\alpha^2 - C_1E_{66}\alpha^2 + B_{22}\beta^2 - C_1E_{22}\beta^2, \\
S_{33} &= A_{55}\alpha^2 - 2C_2D_{55}\alpha^2 + A_{44}\beta^2 - 2C_2D_{44}\beta^2 + C_2^2F_{55}\alpha^2 + C_2^2F_{44}\beta^2 \\
&\quad + 2C_1E_{11}\frac{1}{R_1}\alpha^2 + 2C_1E_{12}\frac{1}{R_2}\alpha^2 + C_1^2H_{11}\alpha^4 + C_1^2H_{12}\alpha^2\beta^2 + 2C_1^2H_{66}\alpha^2\beta^2 + 2C_1E_{12}\frac{1}{R_1}\beta^2 \\
&\quad + 2C_1E_{22}\frac{1}{R_2}\beta^2 + C_1^2H_{12}\alpha^2\beta^2 + C_1^2H_{22}\beta^4 - A_{11}\frac{1}{R_1^2} - 2\frac{1}{R_1R_2}A_{12} - A_{22}\frac{1}{R_2^2}, \\
S_{34} &= S_{43} = A_{55}\alpha - 2C_2D_{55}\alpha + C_2^2F_{55}\alpha - C_1F_{11}\alpha^3 + C_1^2H_{11}\alpha^3 - 2C_1F_{66}\alpha\beta^2 \\
&\quad + 2C_1^2H_{66}\alpha\beta^2 + C_1^2H_{12}\alpha\beta^2 - \frac{1}{R_1}B_{11}\alpha + C_1\frac{1}{R_1}E_{11}\alpha - \frac{1}{R_2}B_{12}\alpha + C_1\frac{1}{R_2}E_{12}\alpha, \\
S_{35} &= S_{53} = A_{44}\beta - 2C_2D_{44}\beta + C_2^2F_{44}\beta - C_1F_{12}\alpha^2\beta + C_1^2H_{12}\alpha^2\beta - 2C_1F_{66}\alpha^2\beta + 2C_1^2H_{66}\alpha^2\beta \\
&\quad - C_1F_{22}\beta^3 + C_1^2H_{22}\beta^3 - \frac{1}{R_1}B_{12}\beta + C_1\frac{1}{R_1}E_{12}\beta - \frac{1}{R_2}B_{22}\beta + C_1\frac{1}{R_2}E_{22}\beta, \\
S_{44} &= D_{11}\alpha^2 - 2C_1F_{11}\alpha^2 + D_{66}\beta^2 - 2C_1F_{66}\beta^2 - A_{55} + 2C_2D_{55} - C_2^2F_{55} + C_1^2H_{11}\alpha^2 + C_1^2H_{66}\beta^2, \\
S_{45} &= S_{54} = D_{66}\alpha\beta + D_{12}\alpha\beta - 2C_1F_{66}\alpha\beta - 2C_1F_{12}\alpha\beta + C_1^2H_{12}\alpha\beta - C_1F_{66}\alpha\beta + C_1^2H_{66}\alpha\beta, \\
S_{55} &= D_{66}\alpha^2 - 2C_1F_{66}\alpha^2 + D_{22}\beta^2 - 2C_1F_{22}\beta^2 - A_{44} + 2C_2D_{44} - C_2^2F_{44} + C_1^2H_{66}\alpha^2 + C_1^2H_{22}\beta^2, \\
C_{13} &= \mathcal{A}_{31}\alpha, & C_{23} &= \mathcal{A}_{32}\beta, & C_{33} &= -\mathcal{C}_{31}\alpha^2 - \mathcal{C}_{32}\beta^2 + \frac{\mathcal{A}_{31}}{R_1} + \frac{\mathcal{A}_{32}}{R_2}, \\
C_{43} &= \mathcal{B}_{31}\alpha - C_1\mathcal{C}_{31}\alpha, & C_{53} &= \mathcal{B}_{32}\beta - C_1\mathcal{C}_{32}\beta, \\
M_{11} &= \bar{I}_1, & M_{12} &= M_{21} = M_{15} = M_{51} = M_{24} = M_{42} = M_{45} = M_{54} = 0, & M_{13} &= M_{31} = \bar{I}_3\alpha, \\
M_{14} &= M_{41} = \bar{I}_2, & M_{22} &= \bar{J}_1, & M_{23} &= M_{32} = \bar{J}_3\beta, & M_{25} &= M_{52} = \bar{J}_2, \\
M_{33} &= \bar{I}_1 + C_1^2I_7(\alpha^2 + \beta^2), & M_{34} &= M_{43} = \bar{I}_5\alpha, & M_{35} &= M_{53} = \bar{J}_5\beta, & M_{44} &= \bar{I}_4, & M_{55} &= \bar{J}_4,
\end{aligned}$$

Table 2. Definition of the variables appearing in Equation (31). The magnetostrictive coefficients \mathcal{A}_{31} , \mathcal{A}_{32} , \mathcal{B}_{31} , \mathcal{B}_{32} , \mathcal{C}_{31} , and \mathcal{C}_{32} are defined in (24).

where S_{ij} , C_{ij} , and M_{ij} ($i, j = 1, 2, \dots, 5$) are defined in Table 2. For vibration control, we assume $q = 0$ and seek the solution of the ordinary differential equations (31) in the form

$$U_{mn}(t) = U_0e^{\lambda t}, \quad V_{mn}(t) = V_0e^{\lambda t}, \quad W_{mn}(t) = W_0e^{\lambda t}, \quad X_{mn}(t) = X_0e^{\lambda t}, \quad Y_{mn}(t) = Y_0e^{\lambda t}. \quad (32)$$

Substituting (32) into (31), and defining

$$\bar{S}_{ij} = S_{ij} + \lambda C_{ij} + \lambda^2 M_{ij} \quad (i, j = 1, 2, 3, 4, 5), \quad (33)$$

we obtain as the condition for a nontrivial solution

$$\begin{vmatrix} \bar{S}_{11} & \bar{S}_{12} & \bar{S}_{13} & \bar{S}_{14} & \bar{S}_{15} \\ \bar{S}_{21} & \bar{S}_{22} & \bar{S}_{23} & \bar{S}_{24} & \bar{S}_{25} \\ \bar{S}_{31} & \bar{S}_{32} & \bar{S}_{33} & \bar{S}_{34} & \bar{S}_{35} \\ \bar{S}_{41} & \bar{S}_{42} & \bar{S}_{43} & \bar{S}_{44} & \bar{S}_{45} \\ \bar{S}_{51} & \bar{S}_{52} & \bar{S}_{53} & \bar{S}_{54} & \bar{S}_{55} \end{vmatrix} = 0. \quad (34)$$

This equation gives five sets of eigenvalues. The lowest one corresponds to the transverse motion. The eigenvalue can be written as $\lambda = -\alpha + i\omega_d$, so that the damped motion is given by

$$u_3(x_1, x_2, t) = \frac{1}{\omega_d} e^{-\alpha t} \sin \omega_d t \sin \frac{n\pi x_1}{a} \sin \frac{n\pi x_2}{b}. \quad (35)$$

In arriving at the last solution, the following boundary conditions are used:

$$\begin{aligned} u_1(x_1, x_2, 0) = 0, \quad \dot{u}_1(x_1, x_2, 0) = 0, \quad u_2(x_1, x_2, 0) = 0, \quad \dot{u}_2(x_1, x_2, 0) = 0, \quad u_3(x_1, x_2, 0) = 0, \\ \dot{u}_3(x_1, x_2, 0) = 1, \quad \phi_1(x_1, x_2, 0) = 0, \quad \dot{\phi}_1(x_1, x_2, 0) = 0, \quad \phi_2(x_1, x_2, 0) = 0, \quad \dot{\phi}_2(x_1, x_2, 0) = 0. \end{aligned} \quad (36)$$

4. Results and discussion

In the present work a theoretical analysis of a functionally graded material (FGM) shell, consisting of layers of magnetostrictive material, is carried out. The magnetostrictive material is assumed to impart vibration control through a velocity dependent feedback law that controls the current to the magnetic coils energizing the magnetostrictive material. Higher order shear deformation theory (HSDT) is used in the derivation. Numerical simulation results are presented. The effect of various parameters on the vibration suppression time is studied. These parameters are: the location of the magnetostrictive layer relative to the neutral plane, the thickness of the magnetostrictive layer, the higher modes of vibration, the material properties of the magnetostrictive material, and the material properties of the FGM material. The influence of HSDT on the vibration response of thick shells is also investigated.

The FGM shell is considered to have dimensions $1 \text{ m} \times 1 \text{ m}$. Two types of FGM shells are considered: FGM1, made up of stainless steel and nickel, and FGM2, made up of nickel and aluminum oxide. The material properties of the constituent materials were listed in [Table 1](#). Two layers of magnetostrictive materials are placed symmetrically away from the neutral plane of the FGM shell, as shown in [Figure 2](#). The magnetostrictive material properties are taken as $E_m = 26.5 \text{ GPa}$, $\nu_m = 0.0$, $\rho_m = 9250 \text{ kg m}^{-3}$, $c(t)r_c = 10^4$. The numerical values of various material and structural constants based on different locations of the magnetostrictive layers and different FGM material properties are listed in [Tables 3](#) and [4](#). In this study, the vibration suppression time (t_s) is defined as the time required to reduce the uncontrolled vibration amplitude to one-tenth of its initial amplitude. In the present numerical simulations the suppression time and the thickness of the magnetostrictive layer are denoted by t_s and h_m , respectively. Z_m represents the distance between the location of the magnetostrictive layer and the neutral plane.

Effect of magnetostrictive layer location. The effect of the location of the magnetostrictive layers on the vibration suppression is studied. [Figure 2](#) shows the location of the magnetostrictive layers in the FGM shells. Transverse deflection values are plotted as functions of time in [Figure 4](#) for several Z_m values: 3.5 mm, 5.5 mm, 7.5 mm and 9.5 mm. For $Z_m = 9.5 \text{ mm}$ [Figure 4d](#) shows the shortest suppression time,

$Z_m/$ m	$F_{11}/$ 10Nm^3	$H_{11}/$ 10^{-3}Nm^5	$D_{11}/$ 10^6Nm	$F_{12}/$ 10Nm^3	$H_{12}/$ 10^{-3}Nm^5	$D_{12}/$ 10^5Nm	$F_{22}/$ 10Nm^3	$H_{22}/$ 10^{-3}Nm^5	$D_{22}/$ 10^6Nm
0.0095	0.624	0.375	0.124	0.178	0.103	0.366	0.624	0.375	0.124
0.0085	0.752	0.534	0.132	0.222	0.157	0.393	0.752	0.534	0.132
0.0075	0.843	0.622	0.139	0.253	0.187	0.417	0.843	0.622	0.139
0.0065	0.904	0.668	0.145	0.274	0.203	0.438	0.904	0.668	0.145
0.0055	0.942	0.689	0.150	0.287	0.210	0.456	0.942	0.689	0.150
0.0045	0.964	0.698	0.155	0.294	0.213	0.471	0.964	0.698	0.155
0.0035	0.976	0.701	0.158	0.298	0.214	0.483	0.976	0.701	0.158
0.0025	0.981	0.702	0.161	0.300	0.215	0.492	0.981	0.702	0.161
0.0015	0.983	0.702	0.163	0.301	0.215	0.498	0.983	0.702	0.163
0.0005	0.983	0.702	0.164	0.301	0.215	0.501	0.983	0.702	0.164
$Z_m/$ m	$F_{66}/$ 10Nm^3	$H_{66}/$ 10^{-3}Nm^5	$D_{66}/$ 10^5Nm	$F_{44}/$ 10Nm^3	$D_{44}/$ 10^5Nm^5	$A_{44}/$ 10^{10}Nm^{-1}	$F_{55}/$ 10Nm^3	$D_{55}/$ 10^5Nm	
0.0095	0.223	0.136	0.438	0.223	0.438	0.156	0.223	0.438	
0.0085	0.265	0.188	0.464	0.265	0.464	0.156	0.265	0.464	
0.0075	0.295	0.217	0.487	0.295	0.487	0.156	0.295	0.487	
0.0065	0.315	0.232	0.507	0.315	0.507	0.156	0.315	0.507	
0.0055	0.328	0.239	0.525	0.328	0.525	0.156	0.328	0.525	
0.0045	0.335	0.242	0.539	0.335	0.539	0.156	0.335	0.539	
0.0035	0.339	0.243	0.551	0.339	0.551	0.156	0.339	0.551	
0.0025	0.340	0.244	0.559	0.340	0.559	0.156	0.340	0.559	
0.0015	0.341	0.244	0.565	0.341	0.565	0.156	0.341	0.565	
0.0005	0.341	0.244	0.568	0.341	0.568	0.156	0.341	0.568	
$Z_m/$ m	$C_1/$ 10^4m^{-2}	$C_2/$ 10^5m^{-2}	$I_1/$ 10^2kgm^{-2}	$I_3/$ 10^{-2}kg	$I_5/$ 10^{-6}kgm^2	$I_7/$ 10^{10}kgm^4	$-\mathcal{B}_{31}/$ 10^2	$-\mathcal{C}_{31}/$ 10^{-2}	
0.0095	0.333	0.100	0.849	0.288	0.175	0.126	0.841	0.761	
0.0085	0.333	0.100	0.849	0.288	0.175	0.126	0.752	0.545	
0.0075	0.333	0.100	0.849	0.285	0.171	0.126	0.664	0.375	
0.0065	0.333	0.100	0.849	0.284	0.170	0.121	0.575	0.244	
0.0055	0.333	0.100	0.849	0.283	0.169	0.120	0.487	0.148	
0.0045	0.333	0.100	0.849	0.282	0.168	0.120	0.398	0.082	
0.0035	0.333	0.100	0.849	0.281	0.168	0.120	0.310	0.039	
0.0025	0.333	0.100	0.849	0.281	0.168	0.120	0.221	0.014	
0.0015	0.333	0.100	0.849	0.280	0.168	0.120	0.133	0.003	
0.0005	0.333	0.100	0.849	0.280	0.168	0.120	0.044	0.000	

Table 3. Coefficients of the FGM1 (stainless steel-nickel) shell.

$Z_m/$ m	$F_{11}/$ 10Nm^3	$H_{11}/$ 10^{-3}Nm^5	$D_{11}/$ 10^6Nm	$F_{12}/$ 10Nm^3	$H_{12}/$ 10^{-3}Nm^5	$D_{12}/$ 10^5Nm	$F_{22}/$ 10Nm^3	$H_{22}/$ 10^{-3}Nm^5	$D_{22}/$ 10^6Nm
0.0095	0.801	0.478	0.161	0.207	0.119	0.426	0.801	0.478	0.161
0.0085	0.974	0.691	0.171	0.258	0.182	0.457	0.974	0.691	0.171
0.0075	1.095	0.809	0.181	0.294	0.218	0.485	1.095	0.809	0.181
0.0065	1.177	0.871	0.189	0.318	0.236	0.509	1.177	0.871	0.189
0.0055	1.228	0.899	0.196	0.333	0.244	0.530	1.228	0.899	0.196
0.0045	1.258	0.911	0.202	0.342	0.248	0.547	1.258	0.911	0.202
0.0035	1.274	0.915	0.207	0.347	0.249	0.561	1.274	0.915	0.207
0.0025	1.281	0.916	0.210	0.349	0.249	0.572	1.281	0.916	0.210
0.0015	1.283	0.916	0.212	0.349	0.249	0.579	1.283	0.916	0.212
0.0005	1.283	0.916	0.214	0.349	0.249	0.583	1.283	0.916	0.214
$Z_m/$ m	$F_{66}/$ 10Nm^3	$H_{66}/$ 10^{-3}Nm^5	$D_{66}/$ 10^5Nm	$F_{44}/$ 10Nm^3	$D_{44}/$ 10^5Nm^5	$A_{44}/$ 10^{10}Nm^{-1}	$F_{55}/$ 10Nm^3	$D_{55}/$ 10^5Nm	
0.0095	0.297	0.179	0.591	0.297	0.591	0.212	0.297	0.591	
0.0085	0.358	0.254	0.628	0.358	0.628	0.212	0.358	0.628	
0.0075	0.401	0.296	0.661	0.401	0.661	0.212	0.401	0.661	
0.0065	0.429	0.317	0.690	0.429	0.690	0.212	0.429	0.690	
0.0055	0.447	0.327	0.715	0.447	0.715	0.212	0.447	0.715	
0.0045	0.458	0.332	0.736	0.458	0.736	0.212	0.458	0.736	
0.0035	0.463	0.333	0.752	0.463	0.752	0.212	0.463	0.752	
0.0025	0.466	0.333	0.765	0.466	0.765	0.212	0.466	0.765	
0.0015	0.467	0.333	0.773	0.467	0.773	0.212	0.467	0.773	
0.0005	0.467	0.333	0.777	0.467	0.777	0.212	0.467	0.777	
$Z_m/$ m	$C_1/$ 10^4m^{-2}	$C_2/$ 10^5m^{-2}	$I_1/$ 10^2kgm^{-2}	$I_3/$ 10^{-2}kg	$I_5/$ 10^{-6}kgm^2	$I_7/$ 10^{10}kgm^4	$-\mathcal{B}_{31}/$ 10^2	$-\mathcal{C}_{31}/$ 10^{-2}	
0.0095	0.333	0.100	0.672	0.240	0.152	0.113	0.841	0.761	
0.0085	0.333	0.100	0.672	0.235	0.144	0.103	0.752	0.545	
0.0075	0.333	0.100	0.672	0.230	0.138	0.097	0.664	0.375	
0.0065	0.333	0.100	0.672	0.226	0.134	0.094	0.575	0.244	
0.0055	0.333	0.100	0.672	0.223	0.131	0.093	0.487	0.148	
0.0045	0.333	0.100	0.672	0.220	0.130	0.092	0.398	0.082	
0.0035	0.333	0.100	0.672	0.218	0.129	0.092	0.310	0.039	
0.0025	0.333	0.100	0.672	0.216	0.129	0.092	0.221	0.014	
0.0015	0.333	0.100	0.672	0.215	0.129	0.092	0.133	0.003	
0.0005	0.333	0.100	0.672	0.215	0.129	0.092	0.044	0.000	

Table 4. Coefficients of the FGM2 (nickel-aluminum oxide) shell.

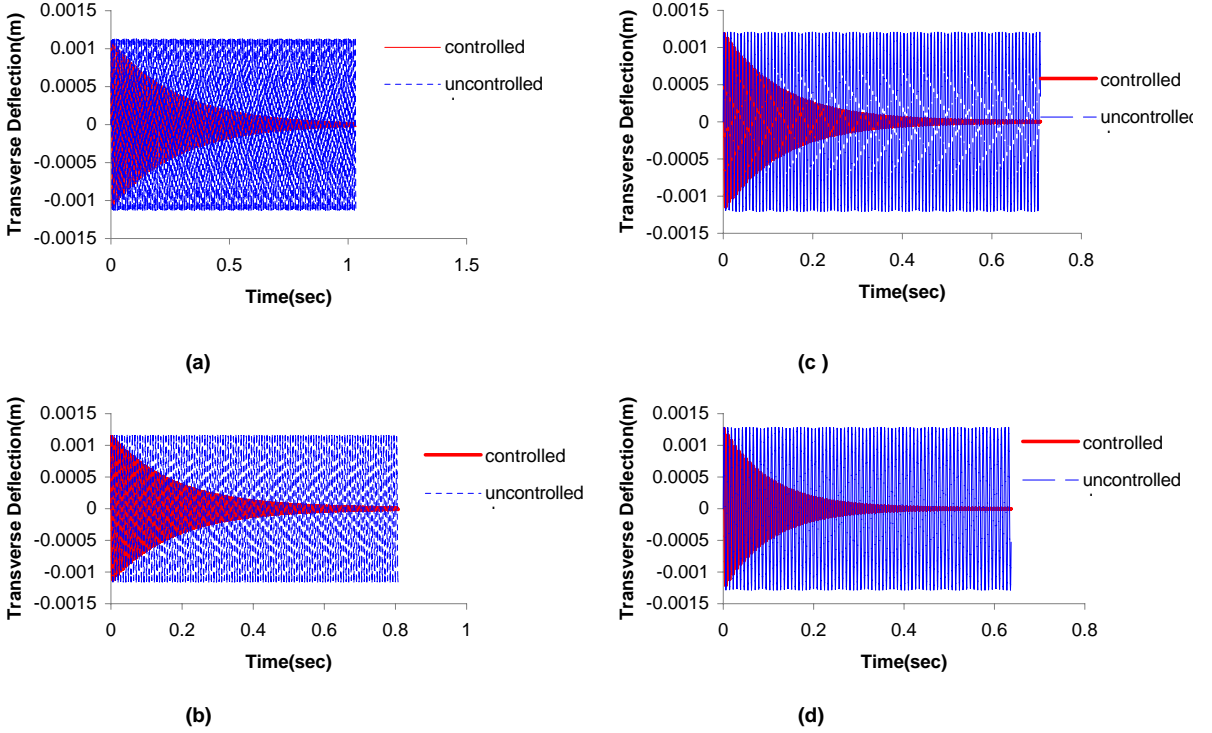


Figure 4. Comparison of uncontrolled (dashed line) and controlled (solid line) motion at the midpoint of the FGM1 shell for various locations of the magnetostrictive layers, (a) $Z_m = 3.5$ mm, (b) $Z_m = 5.5$ mm, (c) $Z_m = 7.5$ mm and (d) $Z_m = 9.5$ mm.

$t_s = 0.22$ s, while for $Z_m = 3.5$ mm [Figure 4a](#) shows the longest suppression time, $t_s = 0.59$ s. From [Figure 4](#), the shortest suppression time is observed when the magnetostrictive layers are placed farther away from the neutral plane. Similarly, from [Figure 4](#) one can observe that the longest suppression time occurs when the magnetostrictive layer is located closest to the neutral plane of the shell.

The influence on the damping of the vibration response of the distance between the magnetostrictive layers and the neutral plane of the shell in the thickness direction is shown in [Tables 5–7](#). In [Tables 5](#) and [6](#), the value of λ_0 increases when the magnetostrictive layer is located farther away from the neutral axis, indicating faster vibration suppression. This is due to the larger bending moment created by the actuating force in the magnetostrictive layers. Further, it is observed that the damping parameter \mathcal{B}_{31} and the associated normalized value of \mathcal{B}_n increase as the magnetostrictive layers are moved away from the neutral plane. These damping parameters are listed in [Tables 3](#) and [4](#). These results agree qualitatively with those presented in [[Pradhan et al. 2001](#); [He et al. 2002](#); [Pradhan 2005](#)].

Effect of thickness of magnetostrictive layers. The vibration response of the FGM1 shell for various thicknesses of the magnetostrictive layers (h_m) is studied. Magnetostrictive damping coefficients and natural frequencies for various thicknesses of the magnetostrictive layers are listed in [Tables 5–6](#). These damping coefficients and natural frequencies refer to the first mode of vibration. The vibration suppression time for h_m values of 1 mm, 2 mm, 3 mm, and 5 mm are listed in [Tables 5](#) and [6](#). These computations

Z_m (m)	$-\lambda_0$	$\pm\omega_d$	W_{\max} (mm)	t_s (s)	t_n
0.0095	9.760	778.57	1.259	0.244	0.055
0.0085	8.731	803.46	1.222	0.268	0.060
0.0075	7.702	828.79	1.184	0.305	0.068
0.0065	6.673	848.44	1.154	0.350	0.078
0.0055	5.645	862.38	1.113	0.410	0.092
0.0045	4.618	873.60	1.116	0.505	0.113
0.0035	3.591	886.54	1.097	0.647	0.145
0.0025	2.564	893.99	1.087	0.909	0.204
0.0015	1.612	892.53	1.091	1.501	0.336
0.0005	0.537	894.26	1.093	4.463	1.000

Z_m (m)	$-\lambda_0$	$\pm\omega_d$	W_{\max} (mm)	t_s (s)	t_n
0.009	18.317	663.54	1.410	0.135	0.118
0.008	16.276	726.37	1.323	0.141	0.124
0.007	14.237	770.68	1.261	0.165	0.145
0.006	12.198	806.39	1.209	0.197	0.173
0.005	10.161	834.35	1.169	0.228	0.200
0.004	8.125	854.79	1.140	0.288	0.252
0.003	6.091	875.41	1.110	0.382	0.335
0.002	4.060	881.40	1.105	0.579	0.507
0.001	2.029	893.62	1.089	1.141	1.000

Z_m (m)	$-\lambda_0$	$\pm\omega_d$	W_{\max} (mm)	t_s (s)	t_n
0.0085	25.702	562.13	1.636	0.092	0.179
0.0075	22.669	661.05	1.401	0.107	0.208
0.0065	19.637	723.98	1.318	0.124	0.241
0.0055	16.607	772.53	1.252	0.140	0.272
0.0045	13.578	812.17	1.196	0.172	0.334
0.0035	10.553	839.35	1.160	0.226	0.439
0.0025	7.533	858.58	1.135	0.309	0.600
0.0015	4.517	881.17	1.104	0.515	1.000

Table 5. Suppression time ratio for various locations of the magnetostrictive layers in the FGM1 shells, for $h_m = 1$ mm (top), $h_m = 2$ mm (middle), and $h_m = 3$ mm (bottom). Z_m is expressed in units of m, W_{\max} in units of mm, and t_s in units of s.

are carried out for various locations (Z_m) of the magnetostrictive layers. The vibration suppression time t_s versus the distance Z_m of the magnetostrictive layers from the neutral plane for various h_m are plotted in Figure 5. This includes magnetostrictive layers with h_m values of 1 mm, 2 mm and 3 mm at various locations. Figure 5 shows that the curve changes more rapidly for a thinner magnetostrictive layer. Further, thin magnetostrictive layers kept away from the neutral plane exhibit better attenuation. The

Z_m	$C(t)r_c = 10^4$					$C(t)r_c = 10^3$				
	$-\lambda_0$	$\pm\omega_d$	W_{\max}	t_s	t_n	$-\lambda_0$	$\pm\omega_d$	W_{\max}	t_s	t_n
0.0075	37.086	414.69	2.071	0.079	0.414	3.709	416.33	2.356	0.623	0.303
0.0065	32.119	565.15	1.594	0.081	0.424	3.212	566.06	1.735	0.724	0.383
0.0055	27.154	669.16	1.377	0.096	0.503	2.715	669.70	1.445	0.856	0.453
0.0045	22.188	743.32	1.282	0.104	0.545	2.219	743.65	1.334	1.024	0.542
0.0035	17.228	792.14	1.219	0.137	0.717	1.723	792.33	1.258	1.303	0.689
0.0025	12.279	831.79	1.168	0.191	1.000	1.228	831.88	1.194	1.890	1.000

Table 6. Suppression time ratio for two values of control gain and various locations of the magnetostrictive layers in the FGM1 shells $h_m = 5$ mm. Z_m is expressed in units of m, W_{\max} in units of mm, and t_s in units of s.

h/a	FSDT		HSDT	
	W_{\max} (mm)	t_s (s)	W_{\max} (mm)	t_s (s)
5	0.085	0.0395	0.129	0.0535
10	0.196	0.0294	0.258	0.0501
100	1.226	0.222	1.259	0.244

Table 7. Vibration suppression using FSDT and HSDT.

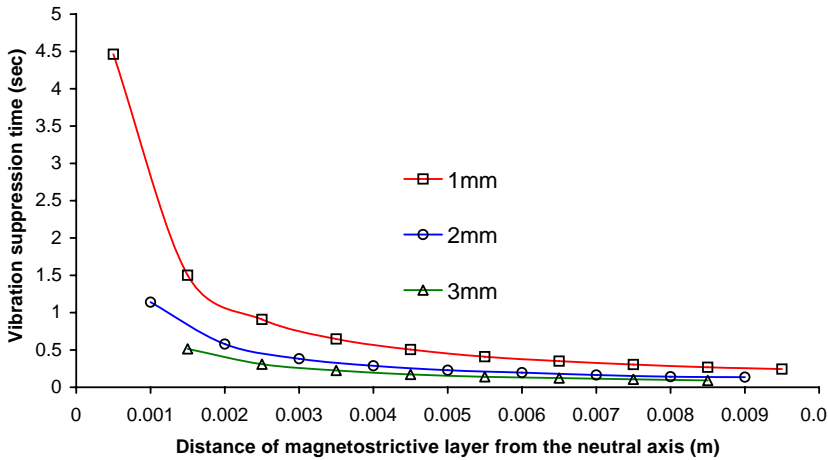


Figure 5. Vibration suppression time (t_s) for various thicknesses of magnetostrictive layers (h_m).

results presented here agree qualitatively with the results presented in [Pradhan et al. 2001; He et al. 2002; Pradhan 2005].

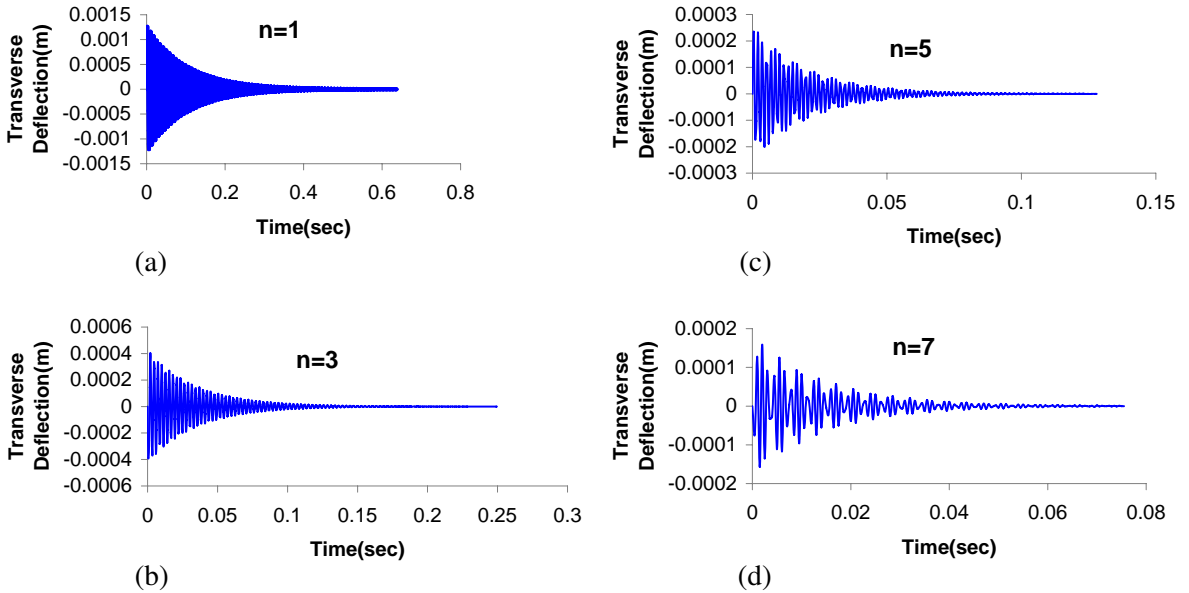


Figure 6. Vibration suppression of higher modes at the midpoint of the FGM1 shell (a) $n = 1$, (b) $n = 3$, (c) $n = 5$, and (d) $n = 7$.

Effect of vibration modes. The effect of higher modes of vibration on the vibration suppression time is studied for the FGM1 shell. Transverse deflection versus time for various cases of the FGM shells are plotted in the next three figures. The parts of Figure 6 show the transient response of modes 1, 3, 5, and 7, respectively. It is observed that attenuation favors the higher modes. This is clearly seen in Figure 7, where modes 1 and 3 are compared for the FGM1 and FGM2 shells. These figures indicate that mode 3 attenuates at a significantly faster rate compared to mode 1. The results in Figure 6 also show that the vibration suppression time decreases very rapidly as the vibration mode number increases. These vibration results for various modes agree qualitatively with the results presented in [Pradhan et al. 2001; Pradhan 2005].

Effect of intensity of control gain. The values of t_s for values of the intensity of control gain $C(t)r_c$ of 1,000 and 10,000 are computed and the results are listed in Table 6. This shows that increase in the intensity of control gain results in a proportional increase in the vibration suppression time. From the results listed in Table 6, it is interesting to note that t_s is directly proportional to the control gain of the applied magnetic field.

Effect of material properties of FGM shell. The effect of the material properties of the FGM shell on the vibration suppression time is studied. Figure 8 displays the vibration suppression for the FGM1 and FGM2 shells. For this comparison study Z_m is assumed to be 9.5 mm. From Figure 8, it is observed that the FGM1 shell has lower frequency compared with the FGM2 shell. This confirms that the FGM1 shell has lower flexural rigidity and thus a lower frequency compared with the FGM2 shell. These results agree qualitatively with the results presented in [Pradhan et al. 2001; Pradhan 2005].

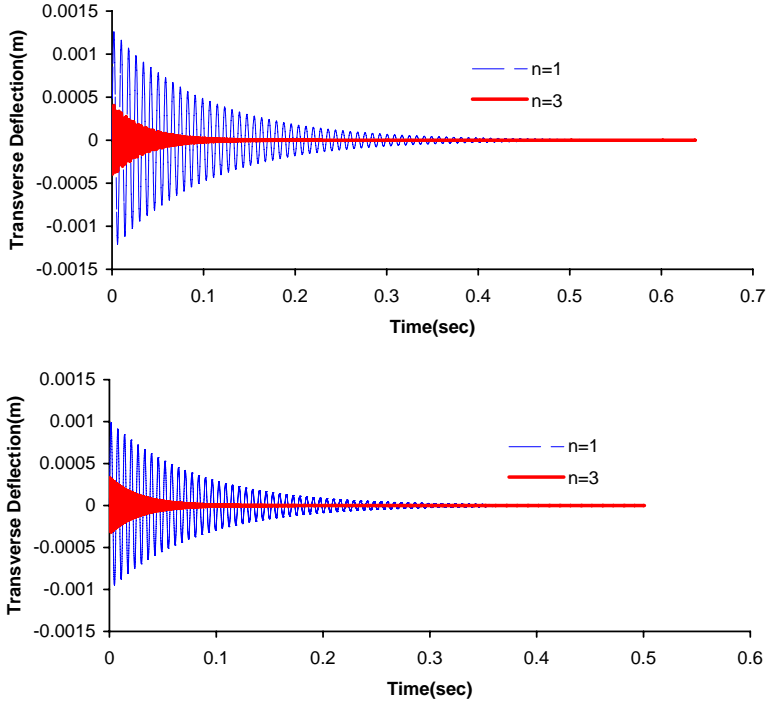


Figure 7. Comparison of controlled motion at the midpoint of the FGM1 (top) and FGM2 (bottom) shells for vibration modes $n = 1$ and $n = 3$.

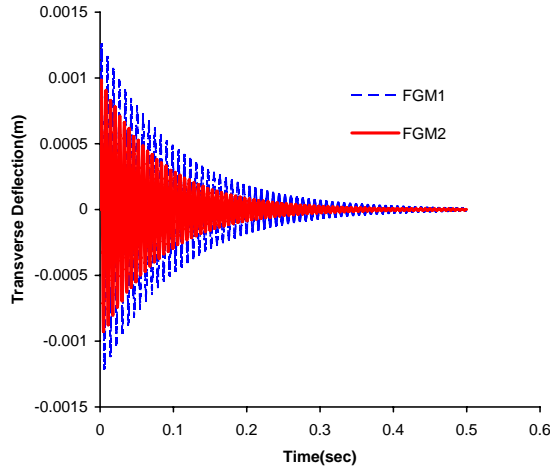


Figure 8. Vibration suppression of the FGM1 and FGM2 shells for $Z_m = 9.5$ mm.

Effect of higher order shear deformation theory. From [Table 6](#), it is observed that when employing HSDT, t_n is dependent on the intensity of the control gain. Under FSDT we observe that t_n is independent of the intensity of the control gain. These results agree qualitatively with the results presented in [\[Pradhan et al. 2001; Pradhan 2005\]](#). t_n is found to depend on the intensity of the control gain. This reveals that

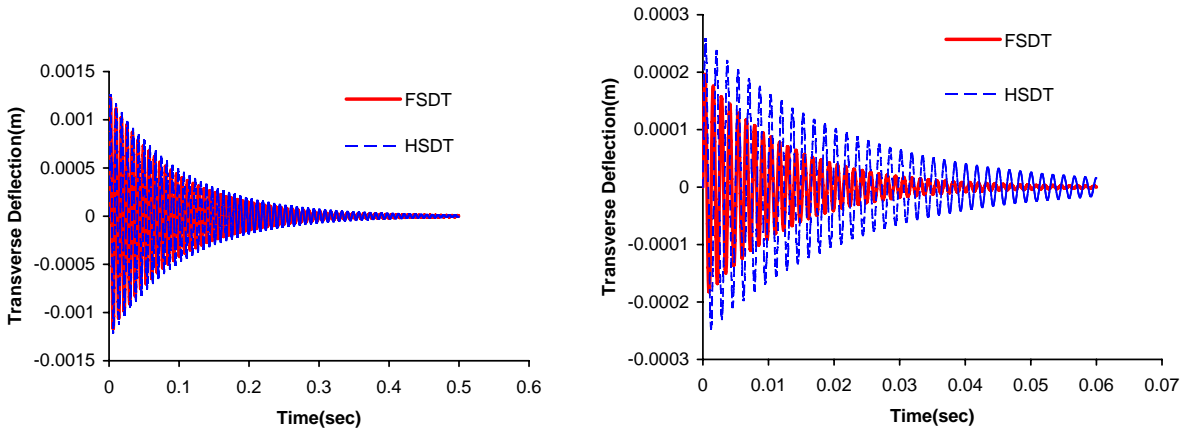


Figure 9. Vibration suppression using FSDT and HSDT for a/h ratios of 100 (left) and 10 (right).

HSDT analysis takes into account the effect of the control gain on the vibration response. Results are obtained for various a/h ratios and listed in Table 7. Here h and a represent the thickness of the shell and the arc length of the shell boundaries. From Table 7 and Figure 9 one could observe that as the thickness of the shell decreases the maximum deflection increases for both FSDT and HSDT. Further maximum deflections predicted by HSDT are larger than those from FSDT. For an a/h ratio of 5 the maximum deflection predicted by HSDT is 51% larger than that from FSDT, while for an a/h ratio of 100 the maximum deflection predicted by HSDT is only 2% larger than that from FSDT. Further, the t_s predicted by HSDT is larger than the corresponding results of FSDT. This is due to the fact that HSDT takes into account the shear forces along the thickness of the thick FGM shell. This study suggests that HSDT should be considered for the analysis of the thick FGM shell.

5. Conclusions

A theoretical formulation for a FGM shell with embedded magnetostrictive layers has been presented. The analytical solutions for the case of simply-supported boundary conditions has been derived, and numerical results are presented. The formulation is based on HSDT, and the analytical solution for the simply-supported shell is based on the Navier solution approach. The effects on the vibration suppression time of the material properties of the FGM shell, the thicknesses of the magnetostrictive layers, and the locations of the magnetostrictive layers have been examined in detail. It was found that attenuation effects were better if the magnetostrictive layers were placed farther away from the neutral plane. Attenuation effects were also better when the magnetostrictive layers were relatively thinner. The suppression time ratio was directly proportional to the control gain of the applied magnetic field. Furthermore, the influence of higher order shear deformation shell theory is significant for thick FGM shells.

Acknowledgement

I am grateful for the technical discussion and suggestions of Professor J. N. Reddy of Texas A&M University.

List of symbols

$A_{31}, A_{32}, B_{31}, B_{32}, C_{31}, C_{32}$	magnetostrictive coefficients
α, β	positive real number
α_1, α_2	surface metrics
$\varepsilon_1, \varepsilon_2, \varepsilon_6, \gamma_4, \gamma_5$	total strains
$\varepsilon_1^0, \varepsilon_2^0, \varepsilon_6^0, \gamma_4^0, \gamma_5^0$	strains from classical shell theory
$\varepsilon_1^1, \varepsilon_2^1, \varepsilon_6^1, \gamma_4^1, \gamma_5^1, \varepsilon_1^2, \varepsilon_2^2, \varepsilon_1^2$	strains from HSDT
ξ_1, ξ_2, ζ	orthogonal curvilinear coordinates
λ	eigenvalue
λ_0	arbitrary constant
ϕ_1, ϕ_2	rotational displacements
ν_1, ν_2	Poisson's ratios of material 1 and material 2
ν_{FGM}	Poisson's ratio of FGM material 1 and material 2
ν_m	Poisson's ratio of magnetostrictive material
$\rho^{(K)}$	density of k -th layer
ρ_m	density of magnetostrictive material
$\sigma_1, \sigma_2, \sigma_4, \sigma_5, \sigma_6$	stress components
ω_d	damping frequency
a	length of the shell
b	breadth of the shell
b_c	coil width
$c(t)$	control gain
dA_1, dA_2	elementary areas across the thickness of the shell
ds	square of the distance on the middle surface
dS	square of the distance
$e_{31}^{(k)}, e_{32}^{(k)}, e_{36}^{(k)}$	magnetostrictive material properties of k -th layer
g_1, g_2	tangents to ξ_1, ξ_2
h	thickness of the shell
h_m	thickness of magnetostrictive layer
k_c	magnetostrictive coil constant
m, m_1, m_2, n	positive integers
n_c	number of coil turns
nm	number of constituent materials in the FGM
q	uniformly distributed load in the transverse direction
r	position vector on the middle surface
r_c	coil radius
t_n	normalized value of t_s
t_s	suppression time ratio
u_1, u_2, u_3	displacements at the middle surface
$\bar{u}_1, \bar{u}_2, \bar{u}_3$	displacements along ξ_1, ξ_2, ζ
z	thickness coordinate

$[\]^0$	contribution due to classical shell theory
$[\]^M$	contribution due to magnetostrictive layer
$A_{ij}, B_{ij}, D_{ij}, E_{ij}, F_{ij}, H_{ij}$	stiffness coefficients of FGM material
C_1, C_2	constants which depend on thickness of the shell
E_1, E_2	Young's moduli of material 1 and material 2
E_{FGM}	Young's modulus of FGM material
E_m	Young's modulus of magnetostrictive material
G_{FGM}	shear modulus of FGM material
H	magnetic field intensity
I	coil current intensity
L_1, L_2, L_3	Lamé coefficients
M^M	moments due to the magnetostrictive layer
N	number of layers assumed for computation
N^M	forces due to the magnetostrictive layer
P_{FGM}	material property of the FGM material
$Q_{ij}^{(k)}$	stiffness coefficients of k -th layer
R	position vector of arbitrary point
R_1, R_2	principal radii of curvature of the middle surface of the shell
R_n	positive real number
S_{ij}, C_{ij}, M_{ij}	coefficients of stiffness, damping and mass matrices
\bar{S}_{ij}	coefficients of solution matrix
V_c	volume fraction of ceramic material
V_{fi}	volume fraction of the constituents of FGM material
V_m	volume fraction of metal material
W_{max}	maximum amplitude in transverse direction
Z_m	transverse location of magnetostrictive layer in the FGM shell

References

[Anjanappa and Bi 1994] M. Anjanappa and J. Bi, “Magnetostrictive mini actuators for smart structure application”, *Smart Mater. Struct.* **3**:4 (1994), 383–390.

[Bryant et al. 1993] M. D. Bryant, B. Fernandez, N. Wang, V. V. Murty, V. Vadlamani, and T. S. West, “Active vibration control in structures using magnetostrictive Terfenol with feedback and/or neural network controllers”, *J. Intell. Mater. Syst. Struct.* **4**:4 (1993), 484–489.

[Friedmann et al. 2001] P. P. Friedmann, G. P. Carman, and T. A. Millott, “Magnetostrictively actuated control flaps for vibration reduction in helicopter rotors: design considerations for implementation”, *Math. Comput. Model.* **33**:10–11 (2001), 1203–1217.

[Giurgiutiu et al. 2001] V. Giurgiutiu, F. Jichi, J. B. Berman, and J. M. Kamphaus, “Theoretical and experimental investigation of magnetostrictive composite beams”, *Smart Mater. Struct.* **10**:5 (2001), 934–945.

[Goodfriend and Shoop 1992] M. J. Goodfriend and K. M. Shoop, “Adaptive characteristics of the magnetostrictive alloy, Terfenol-D, for active vibration control”, *J. Intell. Mater. Syst. Struct.* **3**:2 (1992), 245–254.

[Haddadpour et al. 2007] H. Haddadpour, S. Mahmoudkhani, and H. M. Navazi, “Free vibration analysis of functionally graded cylindrical shells including thermal effects”, *Thin-Walled Struct.* **45**:6 (2007), 591–599.

- [He et al. 2002] X. Q. He, K. M. Liew, T. Y. Ng, and S. Sivashanker, “A FEM model for the active control of curved FGM shells using piezoelectric sensor/actuator layers”, *Int. J. Numer. Methods Eng.* **54**:6 (2002), 853–870.
- [Kadoli and Ganesan 2006] R. Kadoli and N. Ganesan, “Buckling and free vibration analysis of functionally graded cylindrical shells subjected to a temperature-specified boundary condition”, *J. Sound Vib.* **289**:3 (2006), 450–480.
- [Krishna Murty et al. 1997] A. V. Krishna Murty, M. Anjanappa, and Y.-F. Wu, “The use of magnetostrictive particle actuators for vibration attenuation of flexible beams”, *J. Sound Vib.* **206**:2 (1997), 133–149.
- [Li 2008] X.-F. Li, “A unified approach for analyzing static and dynamic behaviors of functionally graded Timoshenko and Euler–Bernoulli beams”, *J. Sound Vib.* **318**:4–5 (2008), 1210–1229.
- [Loy et al. 1999] C. T. Loy, K. Y. Lam, and J. N. Reddy, “Vibration of functionally graded cylindrical shells”, *Int. J. Mech. Sci.* **41**:3 (1999), 309–324.
- [Matsunaga 2009] H. Matsunaga, “Stress analysis of functionally graded plates subjected to thermal and mechanical loadings”, *Compos. Struct.* **87**:4 (2009), 344–357.
- [Pradhan 2005] S. C. Pradhan, “Vibration suppression of FGM shells using embedded magnetostrictive layers”, *Int. J. Solids Struct.* **42**:9–10 (2005), 2465–2488.
- [Pradhan et al. 2000] S. C. Pradhan, C. T. Loy, K. Y. Lam, and J. N. Reddy, “Vibration characteristics of functionally graded cylindrical shells under various boundary conditions”, *Appl. Acoust.* **61**:1 (2000), 111–129.
- [Pradhan et al. 2001] S. C. Pradhan, T. Y. Ng, K. Y. Lam, and J. N. Reddy, “Control of laminated composite plates using magnetostrictive layers”, *Smart Mater. Struct.* **10**:4 (2001), 657–667.
- [Pradyumna and Bandyopadhyay 2008] S. Pradyumna and J. N. Bandyopadhyay, “Free vibration analysis of functionally graded curved panels using a higher-order finite element formulation”, *J. Sound Vib.* **318**:1–2 (2008), 176–192.
- [Reddy 1984a] J. N. Reddy, “A refined nonlinear theory of plates with transverse shear deformation”, *Int. J. Solids Struct.* **20**:9–10 (1984), 881–896.
- [Reddy 1984b] J. N. Reddy, “Exact solutions of moderately thick laminated shells”, *J. Eng. Mech. (ASCE)* **110**:5 (1984), 794–809.
- [Reddy 2004] J. N. Reddy, *Mechanics of laminated composite plates and shells: theory and analysis*, 2nd ed., Chemical Rubber Company, Boca Raton, FL, 2004.
- [Reddy and Liu 1985] J. N. Reddy and C. F. Liu, “A higher-order shear deformation theory of laminated elastic shells”, *Int. J. Eng. Sci.* **23**:3 (1985), 319–330.
- [Woo and Meguid 2001] J. Woo and S. A. Meguid, “Nonlinear analysis of functionally graded plates and shallow shells”, *Int. J. Solids Struct.* **38**:42–43 (2001), 7409–7421.

Received 30 Aug 2008. Revised 7 Jan 2009. Accepted 11 Jan 2009.

SURESH CHANDRA PRADHAN: scp@aero.iitkgp.ernet.in

Department of Aerospace Engineering, IIT Kharagpur, Kharagpur - 721302, West Bengal, India